From histology and imaging data to models for in-stent restenosis

Claudia M. Amatruda[1,2], Carles Bona Casas[3*], Brandis K. Keller[4*], Hannan Tahir[3*], Gabriele Dubini[4], Alfons Hoekstra[3,5], D. Rodney Hose[1,2], Patricia Lawford[1,2], Francesco Migliavacca[4], Andrew Narracott[1,2], Julian Gunn[1,2]*

[1] Medical Physics Group, Department of Cardiovascular Science, University of Sheffield, Sheffield - UK
[2] INSIGNEO Institute for *in Silico* Medicine, University of Sheffield, Sheffield - UK
[3] Computational Science, Institute for Informatics, Faculty of Science, University of Amsterdam, Amsterdam - The Netherlands
[4] LaBS, Department of Chemistry, Materials and Chemical Engineering 'Giulio Natta', Politecnico di Milano, Milan - Italy
[5] National Research University ITMO, Saint-Petersburg - Russian Federation

*These authors contributed equally to this publication

Address for correspondence:
Andrew J. Narracott
Medical Physics Group
Department of Cardiovascular Science
Faculty of Medicine, Dentistry and Health
University of Sheffield
Beech Hill Road
Sheffield S10 2RX, UK
a.j.narracott@sheffield.ac.uk

INTRODUCTION

Percutaneous coronary intervention (PCI), in particular the implantation of stents – slotted tubes expanded in the artery through the inflation of a balloon – has been used to relieve stenoses of the coronary arteries, for several decades (1). Although this technique has proved successful and provides a minimally invasive treatment for

coronary artery disease, for a significant proportion of patients, the long-term outcome following intervention is compromised by restenosis.

Although not completely elucidated, our current understanding is that the stimulus triggering the cascade of events leading to restenosis comes from the vascular injury caused by balloon dilation (barotrauma) and stent placement during PCI. Many biological processes have been proposed to be involved in restenosis including vessel recoil, neointimal proliferation, and early thrombus formation (2-3). The relative contribution of each component to the ultimate extent of restenosis depends on the type of injury.

Coronary stenting virtually eliminates vessel recoil, and in-stent restenosis (ISR) is largely due to neointimal proliferative processes, including vascular smooth muscle cell (VSMC) proliferation and migration, and extracellular matrix formation, resulting in neointimal hyperplasia (4). These events are governed by the elaborate interaction of cellular and molecular responses, including platelet and leukocyte behavior and the coagulation-fibrinolysis system, as well as the secretion of growth factors and pro-inflammatory cytokines (5). In some patients, for particular lesions, the proliferative response is significant enough to result in a clinically significant re-narrowing of the treated vessel. Why this excessive growth of tissue occurs in some lesions and not others is not well understood (2).

Decreased restenosis rates are reported for drug-eluting stents (DES) when compared with bare metal stents (BMS) or balloon angioplasty alone. DES are coated with anti-mitogenic or anti-proliferative drugs to inhibit smooth muscle cell proliferation and neointimal growth but, unfortunately, these too are not without problems. DES are associated with late in-stent thrombosis (IST) and lack of re-endothelialization (6-7). Clinical trials are currently underway to evaluate alternative solutions such as next generation DES (8), drug eluting balloons, (9) and biodegradable vascular scaffolds (10).

The characteristics of stent deployment have been related to the biological response, through investigation of correlations between the depth of stent strut penetration into the vessel wall and the resulting neointimal thickness (11), and stent strut thickness and angiographic restenosis (12). To assess the impact of stent deployment on vascular injury an “injury score” can be derived for each strut. The mean injury score at each cross-section has been shown to be correlated to the neointimal area (11, 13) or percentage stenosis (14). Other predictors of restenosis associated with stent design and deployment (mode of expansion, type, percentage metal coverage, length and strut number, distribution and thickness) have also been reported (15-20).

Although such data provides valuable insight to aid stent design, the exact nature of the association between the local mechanical and fluid dynamic impact of the deployed stent and the biological response of the vessel wall remains unclear. One potential link is local hypoxia. Areas of recirculation local to stent struts and damage to the vasa vasorum may reduce the availability of oxygen to the vessel wall. Recent indications of the correlation between ISR and hypoxia have been elucidated through *in vivo* (21-22), and *in silico* (23) studies.

Animal models provide insights into the mechanisms of ISR and are widely used to evaluate candidate drug inhibitors of ISR (24). Such biological models allow the response of the vessel to stent implantation to be studied without the variability of arteriosclerotic lesion characteristics encountered in patient studies.

This paper brings together results from complementary *in silico* models, describing the methods employed and how their use can improve understanding of the biological response to stenting using a porcine model of restenosis. This process involves the monitoring of the biological response using both imaging and histology and the use of this data to establish numerical models of restenosis. This paper is not intended to provide details of the implementation of each model; for this the reader is referred to relevant publications. An overview of the approach adopted is provided in Figure 1. Such data-driven mathematical modeling will ultimately lead to a deeper insight into the mechanisms of ISR, suggest and inform follow-up studies, and contribute to improved treatment at a population level and, perhaps, even at a patient-specific level. The second section of this paper, “The porcine model of restenosis,” describes the nature of the biological model used to both establish and guide development of the numerical models (Fig. 1a), including the methods used to collect imaging and histology data. The third section, “Spatial variation of ISR stimuli post-stenting,” describes the development of numerical models to examine the relationship between spatial localization of fluid and solid mechanics stimuli immediately post-stenting and the degree of neointimal hyperplasia (Figs. 1b and c). Oxygen mass transport was also modeled. The fourth section, “Analysis of histology data

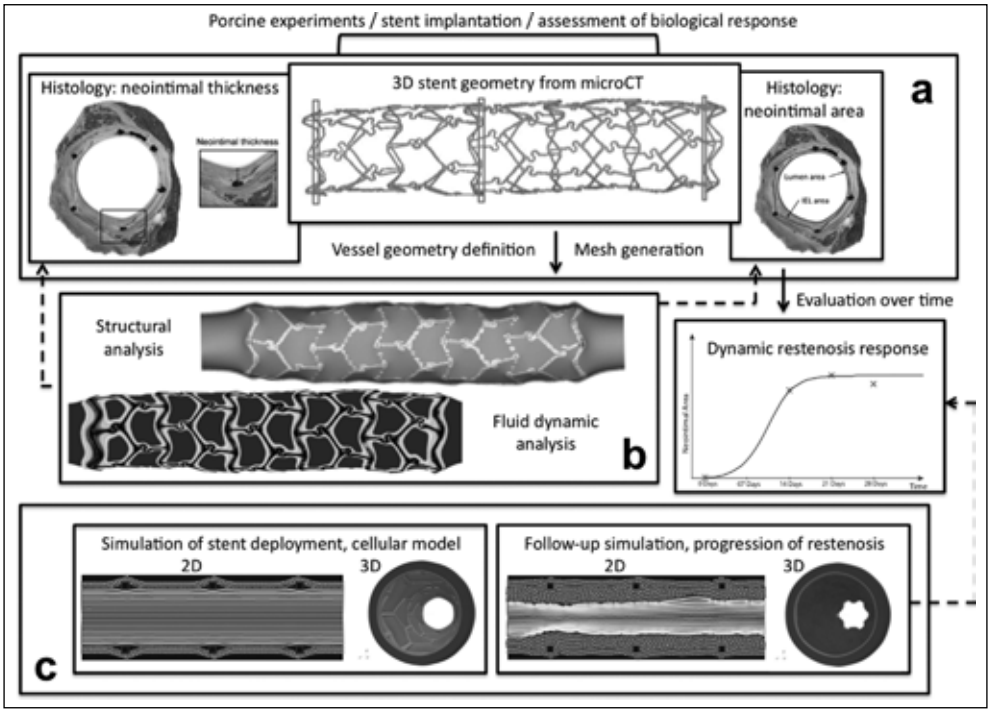

Fig. 1 - *Overview of the workflow for generation and validation of numerical models of restenosis from micro-CT and histology data obtained from a porcine model of restenosis. Solid arrows demonstrate data processing, dashed arrows represent post-processing to inform model behaviour and biological response.* ***(a)*** *Methods used to collect and analyse imaging and histology data.* ***(b)*** *Fluid and solid mechanics models to examine the spatial localization of stimuli immediately post-stenting.* ***(c)*** *Multi-scale models of cellular constituents within the vascular wall to simulate progression of in-stent restenosis.*

to evaluate ISR progression," describes the application of numerical modeling to the study of changes in the stimuli acting on cellular constituents within the vascular wall during the process of neointimal growth (Fig. 1d). Finally, in the fifth section, "Challenges for future research," we outline the challenges that remain to both complete our understanding of the mechanisms responsible for restenosis and translate these models to application in stent design and treatment planning at both population-based and patient-specific levels.

THE PORCINE MODEL OF RESTENOSIS

The development of the numerical models described in this paper is based upon data obtained from a biological model of restenosis. This model has yielded an archive of transverse histological sections derived from over 500 coronary arteries treated with a number of stent designs (25-30). Similar assessment of restenosis in porcine models has been reported by others (31-33). Both Diego et al (33) and Chen et al (31) report evidence to support the finding of Gunn et al (13) that increased stretch in the arterial wall results in greater levels of neointimal growth. Timmins et al (32) report implantation of stents within porcine iliac and femoral arteries, suggesting that greater neointima results from larger differences between the stent-induced stress state and the normal physiological stresses, also supporting the evidence of Gunn et al (13).

This model allows restenosis following stent implantation to be studied by inducing arterial injury through the intentional over-sizing of the stent. As the deployed stent diameter is increased relative to the artery in which it is implanted, more significant arterial injury can be generated, increasing the biological response and degree of restenosis. The animal is sacrificed and the treated artery is removed at a specific time-point post-stenting. To provide the three-dimensional (3D) geometry of the implanted stent, the artery is imaged using a micro-CT scanner. Further details are provided in the next section of this paper. To provide details of the biological response to stenting, the artery is embedded in methacrylate resin and serial cross-sections are cut to allow histological investigation.

Analysis of histology data

Histological studies of the tissues surrounding the stent can provide data on tissue composition (e.g., degree of inflammation, fibrin content) associated with the vascular response to injury following implantation (34). In addition,

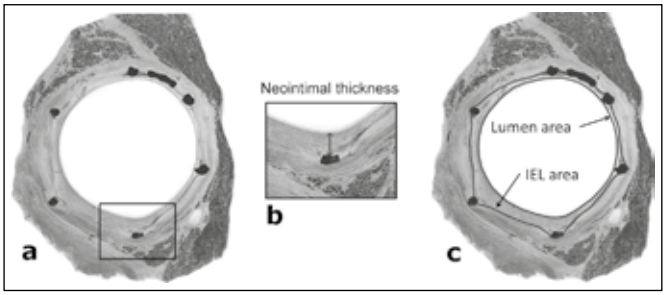

Fig. 2 - a) *Typical histology cross-section;* ***(b)*** *detail of image from (a) showing strut-level neointimal thickness definition;* ***(c)*** *full section showing definition of IEL area and lumen area.*

histomorphometrics yield quantitative information through identification of the internal arterial structures such as the lumen, internal elastic lamina (IEL), and external elastic lamina (EEL).

Figure 2 shows a typical histological section, obtained 14 days after stent implantation and identifies the parameters of interest for the assessment of the magnitude of ISR response. These are:

- neointimal thickness (identified by the length of a line drawn radially between the most internal point of the strut and the edge of the lumen)
- neointimal area (lumen area subtracted from the IEL area)
- percentage restenosis (ratio of lumen area to IEL area).

Detailed study of the variation in histology along the length of the stented artery at both the level of the vessel cross-section and the individual stent strut locations at a single time-point can be used to investigate hypotheses linking the biomechanical environment of the vessel to the biological response, as detailed in the third section of this paper. Since direct measurement of arterial biomechanics at the length-scale of the coronary arteries is challenging, if possible at all, it is necessary to employ modeling techniques to provide a description of the fluid and solid mechanics to explore such hypotheses. Analysis of histological sections obtained from different studies, where the artery is explanted at a number of time-points following stent implantation, allows assessment of trends in the biological response of the vessel wall over time. These issues are described in greater detail in the fourth section in relation to the simulation of the evolution of neointimal tissue development.

SPATIAL VARIATION OF ISR STIMULI POST-STENTING

This section describes the investigation of the relationship between the extent of ISR observed in the porcine model of restenosis and the mechanical stimuli that may play a role in determining the degree of ISR. More precisely, structural mechanics, fluid dynamics, and oxygen transport within a stented artery are reported, neglecting the influence of arterial curvature. For a detailed analysis of the experimental data presented, including arterial curvature, the reader is referred to Keller et al (35), which examines the correlation between structural and fluid mechanics and biological response, and Caputo et al (36), which studies the influence of oxygen transport and fluid dynamics on restenosis.

Combination of 2D histology and 3D stent geometry data

Analysis of serial cross-sections from histology is an effective method for studying the variation of ISR within a stented vessel. However, to provide a detailed description of deployed stent geometry in 3D it is also possible to image the stent using micro-CT. We have previously described a method for combining both histology and stent geometry data to provide a direct comparison between the localization of ISR and realistic deployed stent geometry (37). This is achieved through identification of the axial location of each histology section relative to the 3D stent geometry, using the stent strut positions as landmarks. This approach is demonstrated in Figure 3, which shows both the 3D geometry of the deployed stent, obtained from volumetric micro-CT data, and the corresponding location of a number of histology cross-sections.

When the 3D stent geometry is also used to establish numerical models of the fluid and solid mechanics in the stented artery, as described below, this approach has the significant advantage that the ISR response at the level of both individual cross-sections and individual strut locations can be evaluated for comparison with the local environment within the stented artery.

Numerical simulation of 3D fluid and solid mechanics in the stented artery

Changes in both the solid and fluid mechanics in stented arteries have been linked to the ISR response

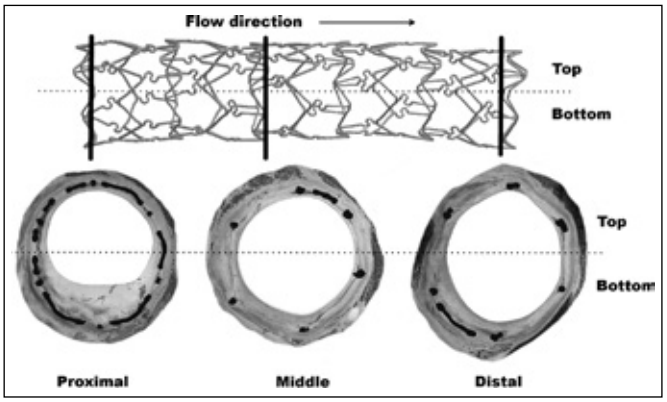

Fig. 3 - *3D geometry of deployed stent obtained from microCT data, solid lines show the axial locations of the histology sections shown below. The histology cross-sections show variation along the stented vessel of strut locations and magnitude of ISR response. The dashed lines illustrate the division into 'top' and 'bottom' sections of the stent used to plot model results in Figure 4.*

post-stenting (38). The presence of the stent increases the stress acting on the vessel wall provoking a chronic injury. This results in the migration of smooth muscle cells towards the lumen (38). Changes in solid mechanics following stenting have been evaluated using finite element techniques to simulate stent/artery interactions and include the generation of high tensile stress within the vessel wall due to stent deployment (32) and von Mises stress under the region of each stent strut (39). Reduced cyclic deformation within the stented region has been linked to increased SMC proliferation and decreased apoptosis *in vitro* using a mock vascular phantom (40). Coronary artery fluid dynamics are significantly altered following the deployment of a stent. This is particularly relevant in the porcine model of restenosis when a stent is deployed within a healthy artery in such a way that the stented segment has a greater diameter than the vessel. The stented region has lower compliance than that of the native artery (41) and the protrusion of the stent struts promotes local regions of recirculation (42).

Due to the small length-scales associated with these variations, computational fluid dynamics (CFD) has been employed as a tool to describe the local hemodynamics of stented arteries. In this way, several candidate parameters have been proposed that identify locations at higher risk of excessive ISR. These parameters include low wall shear stress (WSS<0.5 Pa) and increased oscillatory shear index (OSI values range between 0 when there is no oscillatory WSS to 0.5 when there is maximum oscillatory WSS) (43-44), both of which represent deviations from the physiological values of these parameters within an unstented artery. Shear stresses within the typical physiological range have been shown to decrease endothelial cell expression of VSMC mitogens such as endothelin-1 mRNA (45); while lower flow has been linked to up-regulation of this gene thus promoting extracellular matrix protein production (46). In addition, OSI has been associated with vascular cell rearrangement, and increased endothelial permeability (43).

Changes in solid and fluid mechanics following stent implantation have been studied using data from the porcine model of restenosis as illustrated in Figure 3. A detailed description of the methods employed is provided elsewhere (36), so here we review the approach employed in brief, and present key findings. A BioDivysio™ stainless- steel, balloon-expandable stent (Biocompatibles, Farnham, UK) was implanted in a porcine right coronary artery (RCA) at a stent-artery diameter ratio of 1.4:1, as assessed by quantitative angiography. It was explanted after a period of 14 days and processed into serial sections to assess the ISR response following stent implantation using histology. The 3D stent geometry was reconstructed from micro-CT and the axial location of each histological cross-section was identified as described above. These results are based on the experimental data reported by Morlacchi et al (37), where only fluid dynamics in the proximal region of the stented vessel was considered. Numerical results within the full 3D geometry defined by the deployed stent were used to investigate the variation of solid mechanics, fluid dynamics and oxygen transport within the stented vessel.

The coronary artery was modeled as a cylinder of constant thickness with an initial radius, r, 1.4 mm, measured from angiography before stenting and an arterial wall thickness, h, determined using the ratio $h/2r = 0.04$ (47). ANSYS Mechanical APDL (v14.0) (Ansys, Canonsburg, PA, USA) was used to study the solid mechanics of stent/artery interaction within local regions of axial length 7.5 mm at three locations corresponding to individual histological cross-sections in the proximal, middle, and distal regions of the vessel. Vessel material properties were described using a hyperelastic isotropic material model (48). The vessel was expanded beyond the diameter of the stent using a pressure load (40 MPa) and contact between the stent and vessel lumen was activated as this pressure was removed to capture the stent/artery interaction.

Fluid dynamics and oxygen mass transport simulations were performed on a structural configuration of the stent and vessel surface obtained using an explicit dynamics approach to obtain the boundary of the fluid domain following stent implantation (37). ANSYS CFX v.13.0 (Ansys Inc., Canonsburg, PA, USA) was used to perform fluid dynamic and mass transport simulations under non-pulsatile conditions. The Bird-Carreau constitutive law was used to represent near-wall blood behavior (49). A fully-developed parabolic flow was specified at the inlet, with a no-slip condition at the vessel wall and on the stent, and a zero pressure condition at the outlet.

Following the approach described in (50-53), oxygen transport was modeled using an advection-diffusion equation coupled to blood flow. Convective transport of oxygen within the vessel wall was neglected since transmural velocities are significantly smaller than oxygen diffusion velocities (51). A uniform oxygen concentration was assumed at the inlet and a homogeneous Neumann condition was imposed at the outlet with a value of half the inlet condition assumed at the outer surface of the wall (adventitial surface) based on experimental evidence (54).

Interpretation of 3D fluid and solid mechanics as a stimulus for ISR

Figure 4 shows the variation of compressive stress obtained from the structural model, and the wall shear stress and oxygen concentration obtained from the fluid dynamics model. These can be compared with the localization of neointimal growth, determined by histology, as shown in Figure 3. A greater biological response is observed in the proximal region of the vessel, with a residual lumen of 5.5 mm^2 following the development of neointimal tissue, compared with an IEL area of 10.3 mm^2. This corresponds to a 46.3% stenosis by area. The residual lumen in middle and distal regions of the vessel is larger, corresponding to stenoses of 21.3% and 25.4%, respectively. Higher compressive stresses are observed in the structural analysis toward both proximal and distal limits of the stent, with higher stresses observed on the 'bottom' of the vessel than on the 'top'. A region of reduced wall shear stress is observed at the inlet of the fluid model. This is associated with flow separation due to the increase in vessel diameter caused by the stent deployment. Smaller regions of reduced wall shear stress are observed in the region of each strut. The proximal region of reduced shear stress

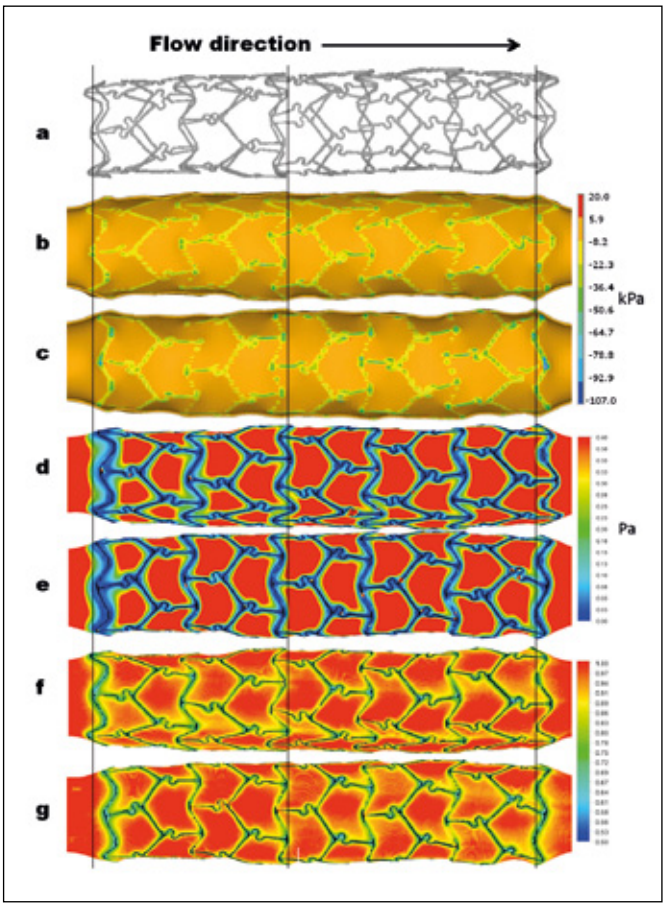

Fig. 4 - ***(a)*** *3D stent geometry. Model results plots showing contours on the inner surface of the vessel;* ***(b), (d), (f)*** *results on the 'top' of the stent;* ***(c), (e), (g)*** *results on the 'bottom' of the stent (see Fig. 3 for definition).* ***(b), (c)*** *Compressive stress contours;* ***(d), (e)*** *wall shear stress contours;* ***(f), (g)*** *oxygen concentration contours. Locations of the histology cross-sections in Figure 3 are identified by solid lines. (d) - (g) are reproduced from (36) with permission.*

corresponds with the localization of neointima in the proximal histology section, as shown in Figure 3. The distribution of oxygen concentration does not demonstrate any significant variation along the length of the stent, except for the local reduction in concentration observed in the region of each stent strut.

These results are consistent with the hypothesis that regions of high stress generated under the struts as a result of contact between the stent and the vessel wall result in a greater biological response through increased vascular injury (55). The results also suggest that a combination of low wall shear stress and high structural stress may amplify the biological response, consistent with the observation that in the proximal region the neointimal response is

greater at the 'bottom' of the stent than at the 'top'. This synergy between fluid dynamics and solid mechanics has been suggested by Chen et al (31), who reported that the product of wall shear stress and tensile stress correlated with neointimal growth in a porcine model using an idealized numerical model of stent deployment. The oxygen plots (Fig. 4), indicate regions of low oxygen concentration adjacent to the strut rings and connectors. If these persist over time they are likely to have an adverse effect on arterial homeostasis; the oxygen supply along the luminal tissue of arteries is considered critical for the metabolic needs of the intima and inner one-third of the artery, with the outer two thirds supplied from the adventitia by means of the vasa vasorum (56). The environment leaves the cells within the inner media under a constant risk of hypoxia and creates increased sensitivity to alterations in oxygen tension and intimal thickening. The results may indicate an association of factors that could influence the tissue healing process and promote the progression of ISR.

A more detailed analysis of the correlation between parameters derived from these *in silico* models and the biological response of the vessel is reported by Caputo et al (36), extending the models to consider the influence of arterial curvature and pulsatile flow. The potential for analysis of the combined influence of these factors to determine the biological response of the vessel and the use of a realistic description of 3D stent geometry to inform generation of the numerical models is demonstrated. The significant benefit of the approach detailed in Figure 1 is that all models, including those described in the following section, are informed by data from a common experimental framework, enhancing the impact of the results from individual modeling approaches on the understanding of stimuli for ISR.

TEMPORAL VARIATION OF ISR STIMULI DURING ISR PROGRESSION

This section describes our investigation of the relationship between the extent of ISR observed in the porcine model of restenosis and the behavior of cellular constituents within the vascular wall and the neointima. A multi-scale simulation framework is presented to describe the evolution of the neointima over time, and the relationship between simulation parameters and biological metrics from histology is described. The aim of these simulations is to establish hypotheses associated with two fundamental questions: Why does ISR start? And why does it stop? By employing *in silico* modeling based on histology from the porcine model we are able to propose and test specific biological mechanisms. In some cases the *in silico* approach is able to exclude or confirm hypotheses, and in other cases the results of simulation can be used to direct future experiments in the porcine model.

Analysis of histology data to evaluate ISR progression

For the assessment of the neointimal response using a single stent design, transverse sections from more than 50 arteries treated with BiodivYsio (Biocompatibles, Farnham, United Kingdom) bare metal stents were evaluated. These sections were harvested at 6 h, 14, 21 and 28 days after the coronary intervention. An average of 10 struts was present in each section. The Gunn injury score (13) was used to quantify the extent of injury at individual struts and the neointimal thickness was measured from the top of each strut (Fig. 2). From this data neointimal thickness was plotted as a function of both the extent of injury and the elapsed time following intervention. Figure 5 shows the mean and standard deviations for a complete set of histological measurements, previously reported by Tahir et al (57).

Multi-scale modeling of ISR progression

The development of a model of ISR is motivated by the desire for a better understanding of the dynamics regulating restenosis. Dynamic modeling of ISR requires a multi-scale multi-science approach (3) coupling a number of single scale models, each representing distinct components of the response. A 2D model of ISR incorporating three single-scale models: blood flow (lattice Boltzmann model), smooth muscle cells (agent-based model) and drug diffusion (based on a finite difference scheme) has been developed and is currently being extended to 3D. Details of the implementation of the single-scale models, their formulation, and mutual coupling can be found in previous publications (3, 57-59); here we provide an overview of the key features of the model.

The definition of the relevant space and time scales associated with ISR and the use of a scale separation map to inform the framework for a multi-scale model of ISR has been described previously (3). The current approach assumes that scale separation between the single-scale

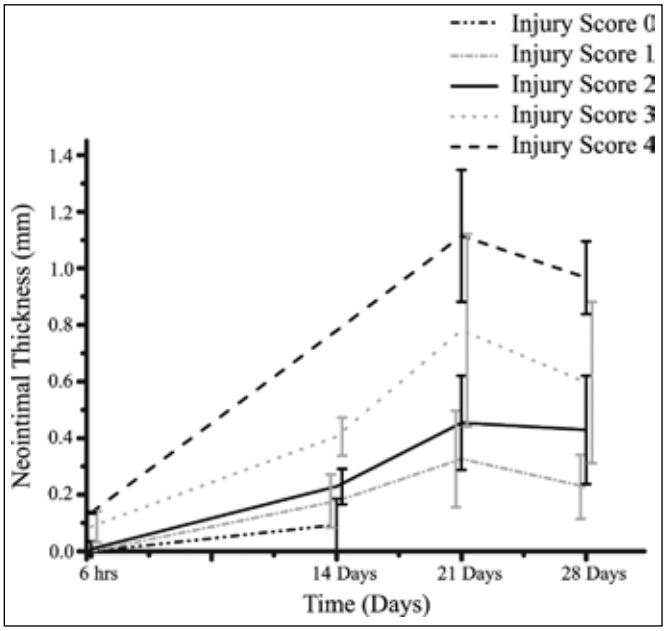

Fig. 5 - *Neointimal thickness as a function of time after stent deployment. The mean and standard deviation of the neointimal measurements are plotted at 6 h, 14, 21, and 28 days post-stent deployment. The data show a positive correlation between neointimal thickness and the Gunn injury scores. Figure reproduced with permission from (57).*

models is confined to the temporal scale. SMC proliferation is identified as the slowest process, dictated by the SMC cell cycle (order 30 h), and blood flow is the fastest process, dictated by the length of one cardiac cycle (order 1 s). However, it is worth noting that scale separation on a spatial scale exists as well within the SMC model itself. The SMC model can be subdivided into processes which occur at the cellular level (order 10 μm), and those occurring at the tissue level (order 1 mm), resulting in a hierarchical multi-scale model.

We have recently reported the application of this multi-scale model of ISR to predict the dynamic response of ISR (57). The model has been used to study the influence of strut shape and size and the dynamic response was characterized by fitting a logistic growth function. Through direct comparison with histology, as described above, the computational output qualitatively predicts the *in vivo* response relating the extent of vascular injury caused by the stent to the degree of neointimal growth. During the initial stage of the response, the model reproduces the *in vivo* observation that the degree of SMC proliferation, and resulting neointima, increases with the degree of injury caused by stent deployment. However, model predictions of the long-term dynamics become unrealistic as all simulations share the same endpoint, a feature which is not observed in the *in vivo* data.

In addition to SMC behavior, the model has been extended to include the process of re-endothelialization following endothelial damage due to balloon inflation and stent deployment. A functional endothelial layer responds to WSS levels by releasing nitric oxide which inhibits SMC growth (60-61). Tahir et al have been able to demonstrate that restenosis may or may not develop, depending on the rates at which re-endothelialization is completed. If restenosis occurs, the amount of neointima directly correlates with the degree of injury caused by the stent, in agreement with the histology (59).

For the 2D simulations presented here, stent deployment is modeled as a separate process to provide an initial condition for the dynamic model of ISR. SMCs start to proliferate as a result of the mechanical insult following stent implantation. The rate of smooth muscle cell proliferation is dependent on the blood flow (specifically WSS) and the number of neighboring SMCs. The blood flow depends on the luminal geometry and thus changes with the proliferation of SMCs.

The initial condition represents the arterial injury caused by the stent by deploying six bare metal stent struts into a 4.5 mm long, 2D artery with a vessel wall thickness of 0.12 mm. The chosen diameter of the lumen prior to stent deployment is 1 mm. The vessel wall is solely composed of densely packed SMCs (media) and an inner lining of internal elastic lamina cells that act as a barrier between the blood and the SMCs. Blood flow is considered to be non-pulsatile. During the stent deployment procedure, stent struts are pushed into the arterial wall, inflicting a structural injury. It is assumed that the pressure exerted by the balloon damages the endothelium and the stent struts cause stretching of the arterial wall that ruptures the IEL layer. In the current model, complete endothelial denudation following stent deployment is assumed. Partial removal of the IEL is based upon the level of longitudinal and hoop stresses imposed by the struts. The partial removal of the IEL represents the amount of injury caused by the stent, which increases with the increase in the deployment depth of the struts (Fig. 6A). After the damage caused by the stent, SMCs from the medial layer become directly exposed to the blood flow and are affected by the altered hemodynamics due to the presence of struts. This allows

phenotype switching in the SMCs from a quiescent contractile state to a more proliferative synthetic state. As the simulation progresses, in parallel with SMC proliferation, damaged endothelium is replaced by the healthy endothelial cells that grow on the innermost layer of the vessel.
The results presented here are obtained by running simulations with two different re-endothelialization scenarios. The first case (rapid endothelial re-growth) is based on data published by Nakazawa et al (62) where a 59% covering of functional endothelium was observed inside the vessel at 3 days post stenting. The percentage of endothelium increased as a function of time until it reached 100% at day 15. The second scenario (a delayed re-endothelialization) is based on our own assumptions and identifies the possible effects of a delay in the appearance of a functional endothelium on the development of ISR. Immediately after stenting, no (0%) endothelium is present and the endothelium re-grows in a linear fashion until it reaches 100% coverage at day 23. To improve our understanding of the dynamic response, for both cases, stent struts were deployed to two different depths (namely, 0.09 mm and 0.13 mm).

Interpretation of results from multi-scale simulations

Figures 6B and 6C show instantaneous representations of the neointimal growth inside the vessel at 28 days post-stenting at a deployment depth of 0.09 mm for both re-endothelialization scenarios. It is clear that a delayed re-appearance of the endothelium results in a greater neointimal response compared to the case of faster re-endothelialization. The variation in neointimal area over time for both re-endothelialization scenarios and both strut deployment depths is shown in Figure 7. This clearly demonstrates that the deeper deployment depth, resulting in greater injury, produces greater neointimal growth and results in a faster growth response (as dictated by the steepness of the curve) for all time-points. This dynamic growth response remains true for both re-endothelialization scenarios.
These results highlight the importance of iterative model development in parallel with analysis and interpretation of biological data. In this case, the histology has driven model development to incorporate an endothelial layer to reproduce the correlation between injury and neointima in the long-term dynamics. However, *in silico* approaches have the potential to direct future biological experiments,

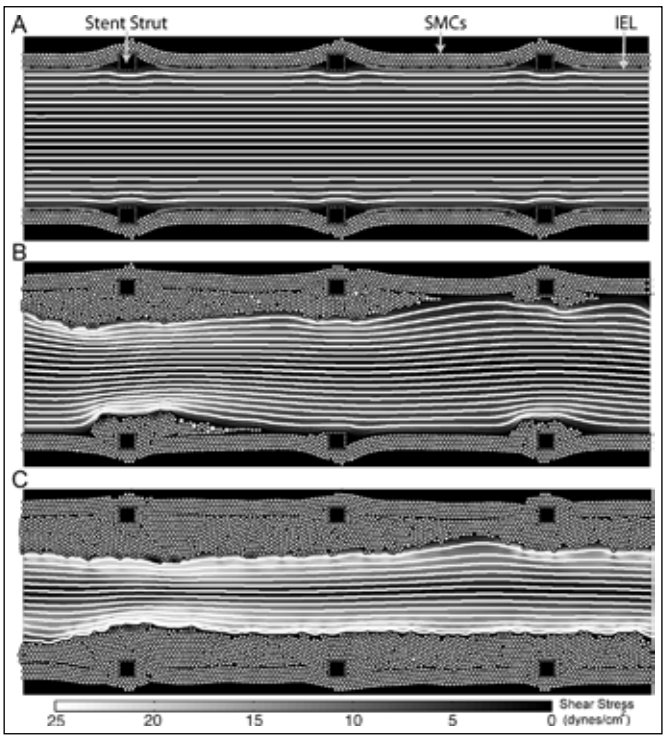

Fig. 6 - *Qualitative comparison of neointimal growth between two endothelialization rates.* ***(A)*** *A benchmark geometry where six BMS struts were deployed at a depth of 90 μm into the tissue. Blood flow is from left to right and streamlines are shown inside the domain. Neointimal growth after 40 days post-stenting with the assumption of a faster endothelium recovery* ***(B)*** *and with delayed endothelium recovery* ***(C)****.*

to provide quantitative comparisons. Additional experiments are required to determine accurate rates of recovery of functional endothelium. There also remains further potential for model development with existing data to capture the decrease in the neointimal thickness measured after 28 days. This response, shown in Figure 5, may be related to vessel remodeling a feature which is not captured in the present computational model.

CHALLENGES FOR FUTURE RESEARCH

This paper has described numerical models employed to study both the localization of mechanical stimuli within stented arteries and the evolution of such stimuli over time during development of neointimal tissue. Through direct comparison with *in vivo* data of the biological response to stent implantation, provided by histology, we are able to examine hypotheses which increase our understanding

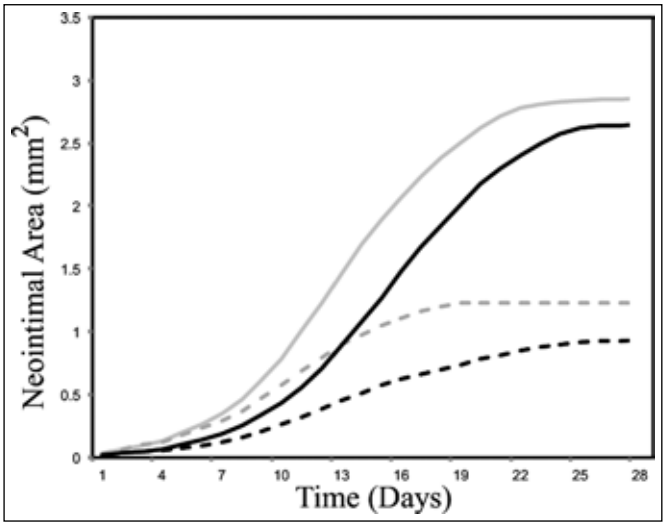

Fig. 7 - *Dynamic response of ISR with the assumption of two re-endothelialization rates and two deployment depths. Simulations result shown in* ***black*** *represents the cases where strut deployment depth was 90 μm, whereas* ***grey*** *shows the results obtained with a deeper deployment depth (130 μm). The dashed lines show the cases where endothelium recovery was faster whereas continuous lines show the results of delayed re-endothelialization.*

of why a greater degree of in-stent restenosis is observed within some stented regions.

However, a significant challenge in modeling biological phenomena is the limited availability of appropriate *in vivo* or *in vitro* data to both inform the establishment of the modeling framework and to validate the outcomes of numerical models. In particular, acceptance of such models by both industrial and clinical end-users is determined by the ability of the models to reproduce biological phenomena consistently and efficiently. This section outlines the challenges for future research in this area addressing issues associated with *in vitro* and *in vivo* experimental data requirements, model enhancements, and translation of models from the controlled context of experimental models of restenosis to application in patient studies.

In vitro experimental data

The experimental data presented in this paper were obtained from an *in vivo* experimental model of restenosis. Such a system reduces the variability of the biology under study, in this case by removing the uncertainty associated with lesion characteristics that would be present in a clinical study. However, significant variation remains in the conditions present in each vessel. Although some of these variations can be accounted for by measurement of the 3D deployed stent geometry, it is challenging to accurately measure all system parameters, such as 3D vascular geometry and wall thickness, and time-dependent fluid boundary conditions. Even if all such parameters could be accurately determined, the complex interaction of stimuli responsible for the biological response makes interpretation of the causal links between physics and biology challenging in such systems.

To address this issue, *in vitro* experimentation is often undertaken to examine specific biological outcomes under controlled stimuli, such as the response of endothelial cells to changes in shear stress (63). The multi-scale models presented in this paper describe the behavior of vascular constituents at the cellular level and how this behavior varies throughout the vascular wall. Dynamic monitoring of smooth muscle and endothelial cell behavior and how this varies with spatial and temporal changes in physical stimuli would provide valuable data to both inform and validate such models. Techniques such as traction force microscopy provide a mechanism to obtain such data in idealized experimental settings (64).

The idealized nature of such experiments can limit the application of the outcomes from such studies within models that aim to reproduce biological behavior in more complex environments. To bridge this gap there is a need for iterative research to provide understanding of the variation of the biological response at incremental levels of complexity. Zahedmanesh and Lally (65) report such an approach applied to the study of SMC behavior within a tissue-engineering scaffold and the variation in cellular response with scaffold compliance under pulsatile pressure loading. It is important for such approaches to maintain a tight coupling between development of the modeling and experimental approach, so that individual model features can be validated through appropriate experimental design.

In vivo experimental data

This study reports methods used to enhance the information that can be obtained from *in vivo* experimental data through the combined analysis of 3D stent geometry provided by microCT, and the biological response of the vascular tissue provided by histology. However, such data can only be obtained following explantation of the stented vessel, which

does not allow assessment of restenosis development over time for a specific case of stent implantation. Techniques have been reported that provide the 3D geometry of both the vessel lumen and vessel wall. These have been used to study the development of restenosis in clinical cases at a small number of time-points (66). A detailed description of the deployed stent geometry cannot be obtained with such methods due to the low spatial resolution of the imaging techniques employed. A combination of the techniques reported within this paper, to provide a detailed description of deployed stent geometry, with serial evaluation of development of neointima in 3D would allow direct comparison of model predictions with biological response on a case-by-case basis, rather than relying on comparisons with averaged data.

However, it is clear that the mathematical models have been able to point to key aspects in the response for which little experimental data exists. Considering the initial response, does ISR initially appear at locations of both high compressive stress and low wall shear stress as suggested by our studies? What is the underlying biological mechanism for this? Considering the final stage of the response, the appearance of a healthy endothelium seems to be key, and the dynamic simulations suggest that the time scales at which a healthy endothelium is established may be significant in determining if ISR appears or not. All these issues require more detailed experimentation with either animal model or controlled *ex vivo* environments. Moreover, the appearance of high resolution imaging modalities such as OCT (67) opens up exciting new ways to study the detail of ISR in model systems. We believe that a close interplay between mathematical modeling and new *in vivo* and *in vitro* techniques is required to significantly improve our understanding of ISR, doing justice to the inherent complexity of this pathology.

Model enhancements

So far, the mathematical models of ISR as presented above have shown qualitative agreement with histological data. As a final test of the current set of models, we intend to integrate the detailed post stenting histology and simulations described above in the section on "Spatial variation of ISR stimuli post-stenting" with the 3D version of the dynamical simulations from the section on "Temporal variation of ISR stimuli during ISR progression." This should demonstrate our capability to compute the ISR response in three dimensions, in a realistic artery geometry. The dynamic model of ISR allows computation of the inhibitory effect of drug-eluting stents; a validation of this capability still needs to be demonstrated. The next logical questions are thus: What can we do with these models in their current form? Should they be improved? And if so, how?

Improved accuracy in the collection of data used to inform model generation has been described above. In addition, the accuracy of descriptions of the physics and biology of restenosis may be improved by further model enhancements. For example, further development of modeling at the cellular level might include representation of intercellular signaling with careful selection from evidence in the literature of the most appropriate signaling pathways (63). However, caution is required in selecting targets for further model development as an increase in complexity of such models across all physical and biological processes is unlikely to aid understanding of the primary determinants of restenosis.

We strongly believe that model improvement should be driven by the availability of experimental or clinical data. But we also believe in the converse: that setting up new experiments should take into account hypotheses that have been suggested and tested in mathematical models. The key role of re-endothelialization is a good example. The dynamic simulations of ISR show that under different scenarios of re-endothelialization, ISR may or may not develop. Therefore, we propose that experiments are designed that study in more detail the appearance of healthy endothelium at the site of the stent. This could lead to a better understanding of why one specific patient develops ISR while another does not.

The combination of modeling approaches reported in this paper presents an opportunity to enhance the fidelity of the modeling framework with little increase in computational cost. Coupling of the finite element approach reported in the section on the spatial variation of ISR stimuli post-stenting to the multi-scale model in the section on the temporal variation would provide a mechanism to improve the representation of the structural mechanics following stent implantation. An approach of this type has been reported by Boyle et al (39) to model neointimal growth through a cellular model based on the damage caused by uniform stent deployment within idealized arterial geometries, obtained by the finite element

method (FEM). Update of a finite element representation of vascular mechanics to include the volumetric growth behavior predicted by this multi-scale model of restenosis has not yet been reported, although finite element methods have been applied to study growth and remodeling in other clinical contexts including development of cerebral aneurysms (68).

Translation to clinical studies

Application to clinical studies includes both the use of modeling to inform patient-specific treatment and the application of modeling to guide population-based development of novel medical devices. Morlacchi and Migliavacca (69) review the state-of-the-art in the application of finite element analysis and computational fluid dynamics to the analysis of stented arteries, which includes the study of arterial bifurcations and complex implantation of multiple stents. This review identifies model validation as a significant challenge to be addressed in the translation of simulation to address clinical problems. Computational cost is also a significant issue, in particular the multi-scale approach described in this paper requires considerable computational resources when extended to consider stent/vessel interactions in 3D. High performance distributed computing infrastructures provide a mechanism to facilitate solution of such complex problems in reasonable timescales as described elsewhere (70-71).

Access to such resources also makes it tractable to consider application of the multi-scale approach to the study of parameter sensitivity within such complex systems. The simulation of biological response over a range of input parameters will allow such models to be used to tailor device design to provide optimal results over the full range of anticipated variation within the population. In order to allow for such population studies, we need to further validate our mathematical models, as discussed above, but we also need to assess the key parameters in our models and their distribution over the population.

Patient-specific analysis using such approaches requires simulations to run within timescales that can be accommodated within the clinical workflow associated with patient treatment. In the case of stenting, these timescales are in the order of hours. Although it is unlikely that multi-scale modeling will find direct application within these contexts, the results of multi-scale simulations can be used to guide development of lower-order models of reduced computational cost.

Moreover, in order to translate the current set of mathematical models to clinical studies requires model validation in the context of human data obtained for ISR. This requires two major steps. First, the models should demonstrate their validity for diseased arteries, since the porcine model system describes the response to injury in initially healthy arteries. This requires application of both *in vivo* experiments and mathematical modeling to the domain of diseased, stenosed arteries. Next, we need sufficient human datasets to allow calibration and validation of the mathematical models. Only then will we be able to take the next step and apply the mathematical models in clinical settings, as suggested above.

CONCLUSIONS

This paper presents modeling techniques used to describe the physics and biology of in-stent restenosis (ISR). The methods employed to inform the definition of these models and interpret model outcomes in the context of biological data obtained from a porcine model of ISR have also been described. The importance of considering the combined influence of structural and fluid dynamic stimuli has been demonstrated through simulation of the environment within a stented artery, using the measured 3D deployed stent geometry to establish the model and histology to quantify the resulting neointimal response. The use of a multi-scale approach to provide a description of both endothelial and smooth muscle cell behavior during neointimal growth has been described. Comparison between the dynamic response of the simulation and data from the porcine model has been used to propose novel experimental questions to be addressed through further experimentation.

Future perspectives for *in vitro* and *in vivo* experimentation to further inform model development have been proposed along with avenues for further model enhancement. The challenges with translation of such approaches to clinical studies for device optimization at the population level or for patient-specific analysis to aid treatment planning have been outlined. These include model validation across a range of levels of complexity and ensuring computational resource requirements do not present a barrier to further application.

Financial Support: The research leading to these results received funding from the European Union Seventh Framework Programme (FP7/2007-2013) under grant agreement no. 238113 – project 'MeD-DiCA', a Network for Initial Training (ITN).

Conflict of Interest: None.

REFERENCES

1. Iqbal J, Gunn J, Serruys PW. Coronary stents: historical development, current status and future directions. Br Med Bull. 2013;106:193-211.
2. Jukema JW, Verschuren JJ, Ahmed TA, Quax PH. Restenosis after PCI. Part 1: pathophysiology and risk factors. Nat Rev Cardiol. 2011;9(1):53-62.
3. Evans DJ, Lawford PV, Gunn J, et al. The application of multiscale modelling to the process of development and prevention of stenosis in a stented coronary artery. Philos Trans A Math Phys Eng Sci. 2008;366(1879):3343-3360.
4. Agema WR, Jukema JW, Pimstone SN, Kastelein JJ. Genetic aspects of restenosis after percutaneous coronary interventions: towards more tailored therapy. Eur Heart J. 2001; 22(22):2058-2074.
5. Lee MS, David EM, Makkar RR, Wilentz JR. Molecular and cellular basis of restenosis after percutaneous coronary intervention: the intertwining roles of platelets, leukocytes, and the coagulation-fibrinolysis system. J Pathol. 2004; 203(4):861-870.
6. Daemen J, Serruys PW. Drug-eluting stent update 2007: part II: Unsettled issues. Circulation. 2007;116(8):961-968.
7. Bavry AA, Kumbhani DJ, Helton TJ, Borek PP, Mood GR, Bhatt DL. Late thrombosis of drug-eluting stents: a meta-analysis of randomized clinical trials. Am J Med. 2006; 119(12):1056-1061.
8. Sabate M, Cequier A, Iñiguez A, et al. Everolimus-eluting stent versus bare-metal stent in ST-segment elevation myocardial infarction (EXAMINATION): 1 year results of a randomised controlled trial. Lancet. 2012;380(9852): 1482-1490.
9. Byrne RA, Neumann FJ, Mehilli J, et al; ISAR-DESIRE 3 investigators. Paclitaxel-eluting balloons, paclitaxel-eluting stents, and balloon angioplasty in patients with restenosis after implantation of a drug-eluting stent (ISAR-DESIRE 3): a randomised, open-label trial. Lancet. 2013;381(9865): 461-467.
10. Diletti R, Serruys PW, Farooq V, et al. ABSORB II randomized controlled trial: a clinical evaluation to compare the safety, efficacy, and performance of the Absorb everolimus-eluting bioresorbable vascular scaffold system against the XIENCE everolimus-eluting coronary stent system in the treatment of subjects with ischemic heart disease caused by de novo native coronary artery lesions: rationale and study design. Am Heart J. 2012;164(5):654-663.
11. Schwartz RS, Huber KC, Murphy JG, et al. Restenosis and the proportional neointimal response to coronary artery injury: results in a porcine model. J Am Coll Cardiol. 1992; 19(2):267-274.
12. Pache J, Kastrati A, Mehilli J, et al. Intracoronary stenting and angiographic results: strut thickness effect on restenosis outcome (ISAR-STEREO-2) trial. J Am Coll Cardiol. 2003; 41(8):1283-1288.
13. Gunn J, Arnold N, Chan KH, Shepherd L, Cumberland DC, Crossman DC. Coronary artery stretch versus deep injury in the development of in-stent neointima. Heart. 2002;88(4):401-405.
14. Kornowski R, Hong MK, Tio FO, Bramwell O, Wu H, Leon MB. In-stent restenosis: contributions of inflammatory responses and arterial injury to neointimal hyperplasia. J Am Coll Cardiol. 1998;31(1):224-230.
15. de Feyter PJ, Kay P, Disco C, Serruys PW. Reference chart derived from post-stent-implantation intravascular ultrasound predictors of 6-month expected restenosis on quantitative coronary angiography. Circulation. 1999;100(17):1777-1783.
16. Foley DP, Pieper M, Wijns W, et al; MAGIC 5L investigators. The influence of stent length on clinical and angiographic outcome in patients undergoing elective stenting for native coronary artery lesions; final results of the Magic 5L Study. Eur Heart J. 2001;22(17):1585-1593.
17. Kitabata H, Kubo T, Komukai K, et al. Effect of strut thickness on neointimal atherosclerotic change over an extended follow-up period (≥4 years) after bare-metal stent implantation: intracoronary optical coherence tomography examination. Am Heart J. 2012;163(4):608-616.
18. Morton AC, Crossman D, Gunn J. The influence of physical stent parameters upon restenosis. Pathol Biol (Paris). 2004; 52(4):196-205.
19. Rogers C, Edelman ER. Endovascular stent design dictates experimental restenosis and thrombosis. Circulation. 1995;91(12):2995-3001.

20. Takebayashi H, Mintz GS, Carlier SG, et al. Nonuniform strut distribution correlates with more neointimal hyperplasia after sirolimus-eluting stent implantation. Circulation. 2004; 110(22):3430-3434.
21. Sanada JI, Matsui O, Yoshikawa J, Matsuoka T. An experimental study of endovascular stenting with special reference to the effects on the aortic vasa vasorum. Cardiovasc Intervent Radiol. 1998;21(1):45-49.
22. Santilli SM, Wernsing SE, Lee ES. Transarterial wall oxygen gradients at a prosthetic vascular graft to artery anastomosis in the rabbit. J Vasc Surg. 2000;31(6):1229-1239.
23. Coppola G, Caro C. Arterial geometry, flow pattern, wall shear and mass transport: potential physiological significance. J R Soc Interface. 2009;6(35):519-528.
24. Lowe HC, Oesterle SN, Khachigian LM. Coronary in-stent restenosis: current status and future strategies. J Am Coll Cardiol. 2002;39(2):183-193.
25. Chamberlain J, Gunn J, Francis S, Holt C, Crossman D. Temporal and spatial distribution of interleukin-1 beta in balloon injured porcine coronary arteries. Cardiovasc Res. 1999;44(1):156-165.
26. Chamberlain J, Gunn J, Francis SE, et al. TGFbeta is active, and correlates with activators of TGFbeta, following porcine coronary angioplasty. Cardiovasc Res. 2001;50(1): 125-136.
27. Chico TJ, Chamberlain J, Gunn J, et al. Effect of selective or combined inhibition of integrins alpha (IIb) beta (3) and alpha (v) beta (3) on thrombosis and neointima after oversized porcine coronary angioplasty. Circulation. 2001;103(8):1135-1141.
28. Dean CJ, Morton AC, Arnold ND, Hose DR, Crossman DC, Gunn J. Relative importance of the components of stent geometry to stretch induced in-stent neointima formation. Heart. 2005;91(12):1603-1604.
29. Morton AC, Arnold ND, Crossman DC, Gunn J. Response of very small (2 mm) porcine coronary arteries to balloon angioplasty and stent implantation. Heart. 2004;90(3):324-327.
30. Morton AC, Arnold ND, Gunn J, et al. Interleukin-1 receptor antagonist alters the response to vessel wall injury in a porcine coronary artery model. Cardiovasc Res. 2005; 68(3):493-501.
31. Chen HY, Sinha AK, Choy JS, et al. Mis-sizing of stent promotes intimal hyperplasia: impact of endothelial shear and intramural stress. Am J Physiol Heart Circ Physiol. 2011; 301(6):H2254-H2263.
32. Timmins LH, Miller MW, Clubb FJ Jr, Moore JE, Jr. Increased artery wall stress post-stenting leads to greater intimal thickening. Lab Invest. 2011;91(6):955-967.
33. Diego A, Pérez de Prado A, Cuellas C, et al. La reestenosis en el stent depende del daño vascular inducido. ¿Son válidos los modelos experimentales actuales de análisis de los stents farmacoactivos? [Instent restenosis related to vessel injury score degree. Are current experimental models valid for drug-eluting stents analysis?]. [Article in Spanish] Rev Esp Cardiol. 2011;64(9):745-751.
34. Edelman ER, Rogers C. Pathobiologic responses to stenting. Am J Cardiol. 1998;81(7A):4E-6E.
35. Keller B, Amatruda C, Hose DR, et al. Contribution of Mechanical and Fluid Stresses to the Magnitude of Instent Restenosis at the Level of Individual Stent Struts. Cardiovasc Eng Technol. 2014/02/26 2014:1-12.
36. Caputo M, Chiastra C, Cianciolo C, et al. Simulation of oxygen transfer in stented arteries and correlation with in-stent restenosis. Int J Numer Method Biomed Eng. 2013;29(12): 1373-1387.
37. Morlacchi S, Keller B, Arcangeli P, et al. Hemodynamics and in-stent restenosis: micro-CT images, histology, and computer simulations. Ann Biomed Eng. 2011;39(10):2615-2626.
38. Duraiswamy N, Schoephoerster RT, Moreno MR, Moore JE. Stented Artery Flow Patterns and Their Effects on the Artery Wall. Annu Rev Fluid Mech. 2007;39(1):357-382.
39. Boyle CJ, Lennon AB, Prendergast PJ. Application of a mechanobiological simulation technique to stents used clinically. J Biomech. 2013;46(5):918-924.
40. Colombo A, Guha S, Mackle JN, Cahill PA, Lally C. Cyclic strain amplitude dictates the growth response of vascular smooth muscle cells *in vitro*: role in in-stent restenosis and inhibition with a sirolimus drug-eluting stent. Biomech Model Mechanobiol. 2013;12(4):671-683.
41. Selvarasu NK, Tafti DK, Vlachos PP. Hydrodynamic effects of compliance mismatch in stented arteries. J Biomech Eng. 2011;133(2):021008.
42. Jiménez JM, Davies PF. Hemodynamically driven stent strut design. Ann Biomed Eng. 2009;37(8):1483-1494.
43. Malek AM, Alper SL, Izumo S. Hemodynamic shear stress and its role in atherosclerosis. JAMA. 1999;282(21): 2035-2042.
44. Murphy J, Boyle F. Predicting neointimal hyperplasia in stented arteries using time-dependant computational fluid dynamics: a review. Comput Biol Med. 2010;40(4):408-418.
45. Malek A, Izumo S. Physiological fluid shear stress causes downregulation of endothelin-1 mRNA in bovine aortic endothelium. Am J Physiol. 1992;263(2 Pt 1):C389-C396.
46. Yoshizumi M, Kurihara H, Sugiyama T, et al. Hemodynamic shear stress stimulates endothelin production by cultured endothelial cells. Biochem Biophys Res Commun. 1989; 161(2):859-864.
47. Nichols WW, O'Rourke MF. McDonald's blood flow in arteries: theoretical, experimental, and clinical principles. Boca Raton: CRC Press; 2011.
48. Gijsen FJ, Migliavacca F, Schievano S, et al. Simulation of stent deployment in a realistic human coronary artery. Biomed Eng Online. 2008;7:23.
49. Seo T, Schachter LG, Barakat AI. Computational study of fluid mechanical disturbance induced by endovascular stents. Ann Biomed Eng. 2005;33(4):444-456.
50. Rappitsch G, Perktold K. Computer simulation of convective diffusion processes in large arteries. J Biomech. 1996; 29(2):207-215.

51. Moore JA, Ethier CR. Oxygen mass transfer calculations in large arteries. J Biomech Eng. 1997;119(4):469-475.
52. Quarteroni A, Veneziani A, Zunino P. Mathematical and numerical modeling of solute dynamics in blood flow and arterial walls. SIAM J Numer Anal. 2001;39(5):1488-1511.
53. Quarteroni A, Veneziani A, Zunino P. A domain decomposition method for advection-diffusion processes with application to blood solutes. SIAM J Sci Comput. 2002;23(6):1959-1980.
54. Buerk DG, Goldstick TK. Arterial wall oxygen consumption rate varies spatially. Am J Physiol. 1982;243(6):H948-H958.
55. Boyle CJ, Lennon AB, Early M, Kelly DJ, Lally C, Prendergast PJ. Computational simulation methodologies for mechanobiological modelling: a cell-centred approach to neointima development in stents. Philos Trans A Math Phys Eng Sci. 2010;368(1921):2919-2935.
56. Chisolm GM, Gainer JL, Stoner GE, Gainer JV, Jr. Plasma proteins, oxygen transport and atherosclerosis. Atherosclerosis. 1972;15(3):327-343.
57. Tahir H, Hoekstra AG, Lorenz E, et al. Multi-scale simulations of the dynamics of in-stent restenosis: impact of stent deployment and design. Interface Focus. 2011;1(3):365-373.
58. Caiazzo A, Evans D, Falcone J-L, et al. A Complex Automata approach for in-stent restenosis: Two-dimensional multiscale modelling and simulations. J Comput Sci. 2011;2(1):9-17.
59. Tahir H, Bona-Casas C, Hoekstra AG. Modelling the effect of a functional endothelium on the development of in-stent restenosis. PLoS One. 2013;8(6):e66138.
60. Jeremy JY, Rowe D, Emsley AM, Newby AC. Nitric oxide and the proliferation of vascular smooth muscle cells. Cardiovasc Res. 1999;43(3):580-594.
61. Ahanchi SS, Tsihlis ND, Kibbe MR. The role of nitric oxide in the pathophysiology of intimal hyperplasia. J Vasc Surg. 2007;45 Suppl A:A64-73.
62. Nakazawa G, Granada JF, Alviar CL, et al. Anti-CD34 antibodies immobilized on the surface of sirolimus-eluting stents enhance stent endothelialization. JACC Cardiovasc Interv. 2010;3(1):68-75.
63. Van der Heiden K, Gijsen FJ, Narracott A, et al. The effects of stenting on shear stress: relevance to endothelial injury and repair. Cardiovasc Res. 2013;99(2):269-275.
64. Tambe DT, Hardin CC, Angelini TE, et al. Collective cell guidance by cooperative intercellular forces. Nat Mater. 2011;10(6):469-475.
65. Zahedmanesh H, Lally C. A multiscale mechanobiological modelling framework using agent-based models and finite element analysis: application to vascular tissue engineering. Biomech Model Mechanobiol. 2012;11(3-4):363-377.
66. Wentzel JJ, Krams R, Schuurbiers JC, et al. Relationship between neointimal thickness and shear stress after Wallstent implantation in human coronary arteries. Circulation. 2001;103(13):1740-1745.
67. Cheng KH, Sun C, Cruz JP, et al. Comprehensive data visualization for high resolution endovascular carotid arterial wall imaging. J Biomed Opt. 2012;17(5):056003.
68. Ho H, Suresh V, Kang W, Cooling MT, Watton PN, Hunter PJ. Multiscale modeling of intracranial aneurysms: cell signaling, hemodynamics, and remodeling. IEEE Trans Biomed Eng. 2011;58(10):2974-2977.
69. Morlacchi S, Migliavacca F. Modeling stented coronary arteries: where we are, where to go. Ann Biomed Eng. 2013;41(7):1428-1444.
70. Groen D, Borgdorff J, Bona-Casas C, et al. Flexible composition and execution of high performance, high fidelity multiscale biomedical simulations. Interface Focus. 2013;3(2):20120087.
71. Borgdorff J, Bona-Casas C, Mamonski M, et al. A Distributed Multiscale Computation of a Tightly Coupled Model Using the Multiscale Modeling Language. Procedia Computer Science. 2012;9(0):596-605.